Influence of Interfacial Delamination on Channel Cracking of Elastic Thin Films

Haixia Mei, Yaoyu Pang, Rui Huang

Department of Aerospace Engineering and Engineering Mechanics, University of Texas, Austin, TX 78712 (email: ruihuang@mail.utexas.edu)

Abstract

Channeling cracks in brittle thin films have been observed to be a key reliability issue for advanced interconnects and other integrated structures. Most theoretical studies to date have assumed no delamination at the interface, while experiments have observed channel cracks both with and without interfacial delamination. This paper analyzes the effect of interfacial delamination on the fracture condition of brittle thin films on elastic substrates. It is found that, depending on the elastic mismatch and interface toughness, a channel crack may grow with no delamination, with a stable delamination, or with unstable delamination. For a film on a relatively compliant substrate, a critical interface toughness is predicted, which separates stable and unstable delamination. For a film on a relatively stiff substrate, however, a channel crack grows with no delamination when the interface toughness is greater than a critical value, while stable delamination along with the channel crack is possible only in a small range of interface toughness for a specific elastic mismatch. An effective energy release rate for the steady-state growth of a channel crack is defined to account for the influence of interfacial delamination on both the fracture driving force and the resistance, which can be significantly higher than the energy release rate assuming no delamination.

Key words: channel cracking, delamination, thin films, interface.

1. Introduction

Integrated structures with mechanically soft components have recently been pursued over a wide range of novel applications, from high performance integrated circuits in microelectronics (Ho et al., 2004) to unconventional organic electronics (Dodabalapur, 2006) and stretchable electronics (Wagner et al., 2004; Khang et al., 2006), along with the ubiquitous integration of hard and soft materials in biological systems (Gao, 2006). In particular, the integration of low dielectric constant (low k) materials in advanced interconnects of microelectronics has posed significant challenges for reliability issues resulting from the compromised mechanical properties. Two failure modes have been reported, one for cohesive fracture (Liu et al., 2004) and the other for interfacial delamination (Liu et al., 2007). The former pertains to the brittleness of the low-k materials subjected to tension, and the latter manifests due to poor adhesion between low-k and surrounding materials (Tsui et al., 2006). This paper considers concomitant cohesive fracture and interfacial delamination as a hybrid failure mode in integrated thin-film structures.

One common cohesive fracture mode for thin films under tension is channel cracking (Figure 1). Previous studies have shown that the driving force (i.e., the energy release rate) for the steady-state growth of a channel crack depends on the constraint effect of surrounding layers (Hutchinson and Suo, 1992). For a brittle thin film on an elastic substrate, the driving force increases for increasingly compliant substrates (Beuth, 1992; Huang et al., 2003). The effect of constraint can be partly lost as the substrate deforms plastically (Ambrico and Begley, 2002) or viscoelastically (Huang et al., 2002; Suo et al., 2003). More recent studies have focused on the effects of stacked buffer layers (Tsui et al., 2005; Cordero et al, 2007) and patterned film structures (Liu et al., 2004). In most of these studies, the interfaces between the film and the substrate or the buffer layers are assumed to remain perfectly bonded as the channel crack grows

in the film (Figure 1a). However, the stress concentration at the root of the channel crack may drive interfacial delamination (Ye et al., 1992). While some experimental observations clearly showed no delamination (Tsui et al., 2005; He, et al. 2004), others observed delamination of the interface (Tsui et al., 2005; Suo, 2003). There are two questions yet to be answered: *First, under what condition would the growth of a channel crack be accompanied by interfacial delamination? Second, how would the interfacial delamination (if occurring) affect the fracture condition or reliability in integrated thin film structures?* To answer these questions, this paper considers steady-state channel cracking of an elastic thin film on an elastic substrate and theoretically examines the effect of concomitant interfacial delamination. Section 2 briefly reviews the concept of steady-state driving force for a channel crack growing without delamination. Section 3 analyzes interfacial delamination emanating from the root of a long, straight channel crack. In Section 4, the fracture driving force for the steady-state growth of a channel crack with interfacial delamination is determined. A finite element model is used to calculate the energy release rates for both the interfacial delamination and the steady-state channel cracking. Moreover, to account for the influence of interfacial delamination on the fracture resistance, we define an effective energy release rate that depends on the interface toughness as well as the elastic mismatch between the film and the substrate. In conclusion, Section 5 summarizes the findings and emphasizes the impact of interfacial delamination on the reliability of integrated structures with mechanically soft components.

2. Channel cracking without delamination

As illustrated in Figure 1a, assuming no interfacial delamination, the energy release rate for the steady-state growth of a channel crack in a thin elastic film bonded to a thick elastic substrate is (Beuth, 1992; Hutchinson and Suo, 1992):

$$G_{ss} = Z(\alpha,\beta)\frac{\sigma_f^2 h_f}{\overline{E}_f}, \tag{1}$$

where σ_f is the tensile stress in the film, h_f is the film thickness, and $\overline{E}_f = E_f \big/ \left(1-\nu_f^2\right)$ is the plane strain modulus of the film with Young's modulus E_f and Poisson's ratio ν_f. The dimensionless coefficient Z depends on the elastic mismatch between the film and the substrate, through the Dundurs' parameters

$$\alpha = \frac{\overline{E}_f - \overline{E}_s}{\overline{E}_f + \overline{E}_s} \text{ and } \beta = \frac{\overline{E}_f(1-\nu_f)(1-2\nu_s) - \overline{E}_s(1-\nu_s)(1-2\nu_f)}{2(1-\nu_f)(1-\nu_s)\left(\overline{E}_f + \overline{E}_s\right)}. \tag{2}$$

When the film and the substrate have identical elastic moduli, we have $\alpha = \beta = 0$ and $Z = 1.976$. The value of Z decreases slightly for a compliant film on a relatively stiff substrate ($\overline{E}_f < \overline{E}_s$ and $\alpha < 0$). A more compliant substrate ($\alpha > 0$), on the other hand, provides less constraint against film cracking. Thus, Z increases as α increases. For very compliant substrates (e.g., organic low-k dielectrics, polymers, etc.), Z increases rapidly, with $Z > 30$ for $\alpha > 0.99$ (Beuth, 1992; Huang et al., 2003). The effect of β is secondary and often ignored.

In general, the steady-state energy release rate of channel cracking can be calculated from a two-dimensional (2D) model (Beuth, 1992; Huang et al., 2003) as follows:

$$G_{ss} = \frac{1}{2h_f}\int_0^{h_f} \sigma_f \delta(z)dz, \tag{3}$$

where $\delta(z)$ is the opening displacement of the crack surfaces far behind the channel front (see Fig. 1a). Due to the constraint by the substrate, the crack opening does not change as the channel front advances and the energy release rate attains a steady state, independent of the channel length. Three-dimensional analyses have shown that the steady state is reached when the length of a channel crack exceeds two to three times the film thickness for a relatively stiff substrate (Nakamura and Kamath, 1992), but the crack length to reach the steady state can be significantly longer for more compliant substrate materials (Ambrico and Begley, 2002). The present study focuses on the steady state.

3. Interfacial delamination from channel root

Now consider an interfacial crack emanating from the root of a channel crack at each side (Figure 1b). For a long, straight channel crack, we assume a steady state far behind the channel front, where the interfacial crack has a finite width, *d*. The energy release rate for the interfacial crack can be written in a similar form as Eq. (1):

$$G_d = Z_d\left(\frac{d}{h_f}, \alpha, \beta\right)\frac{\sigma_f^2 h_f}{\overline{E}_f}, \tag{4}$$

where Z_d is a dimensionless function that can be determined from a two-dimensional plane strain problem as illustrated in Figure 2a. In the present study, a finite element model is constructed to calculate the interfacial energy release rate. By symmetry, only half of the film/substrate structure is modeled along with proper boundary conditions (Figure 2b). The finite element package ABAQUS is employed and an example mesh near the interfacial crack is shown in Figure 2c. Close to the tip of the interfacial crack, a very fine mesh is used (Figure 2d), with a set of singular elements around the crack tip. Far away, infinite elements are used for both the film

and substrate to eliminate possible size effects of the model. The method of J-integral is adopted for the calculation of the interfacial energy release rate. In all calculations, we set $\nu_f = \nu_s = \frac{1}{3}$ such that $\beta = \alpha/4$, while the mismatch parameter α is varied.

The dimensionless coefficient Z_d is determined by normalization of the numerical results according to Eq. (4), which is plotted in Figure 3 as a function of the normalized delamination width, d/h_f, for different elastic mismatch parameters. The Z_d function has two limits. First, when $d/h_f \to \infty$ (long crack limit), the interfacial crack reaches a steady state with the energy release rate

$$G_{ss}^{d} = \frac{\sigma_f^2 h_f}{2\bar{E}_f}, \tag{5}$$

and thus $Z_d \to 0.5$. The steady-state energy release rate for the interfacial crack is independent of the crack length as well as the elastic mismatch. On the other hand, when $d/h_f \to 0$ (short crack limit), the interfacial energy release rate follows a power law (He and Hutchinson, 1989a):

$$Z_d \sim \left(\frac{d}{h_f}\right)^{1-2\lambda}, \tag{6}$$

where λ depends on the elastic mismatch and can be determined by solving the equation (Zak and Williams, 1963)

$$\cos\lambda\pi = \frac{2(\beta-\alpha)}{1+\beta}(1-\lambda)^2 + \frac{\alpha+\beta^2}{1-\beta^2}. \tag{7}$$

More details about the solution at the short crack limit as well as comparisons with the finite element results are given in the Appendix. Here we discuss three scenarios at the short crack limit, which would eventually determine the condition for channel cracking with or without

interfacial delamination. First, when $\alpha = \beta = 0$ (no elastic mismatch), we have $\lambda = 0.5$. In this case, Z_d approaches a constant as $d/h_f \to 0$. As shown in the Appendix, an analytical solution predicts that $Z_d(0,0,0) \to 0.9878$, which compares well with our numerical results (Figure A2). When $\alpha > 0$ ($\beta = \alpha/4$), we have $\lambda > 0.5$. Consequently, $Z_d \to \infty$ as $d/h_f \to 0$. As shown in Figure 3, for both $\alpha = 0$ and $\alpha > 0$, the interfacial energy release rate monotonically decreases as the delamination width increases. On the other hand, when $\alpha < 0$, we have $0 < \lambda < 0.5$, and thus, $Z_d \to 0$ as $d/h_f \to 0$. Interestingly, the numerical results in Figure 3 show that, instead of a monotonic variation with respect to the crack length, the interfacial energy release rate oscillates between the short and long crack limits for the cases with $\alpha < 0$. Such an oscillation leads to local maxima of the interfacial energy release rate, which in some cases (e.g., $\alpha = -0.6$) can be greater than the steady state value at the long crack limit.

Previously, Ye et al. (1992) gave an approximate formula for the Z_d function based on their finite element calculations. Although the formula has similar asymptotic limits for long and short cracks as the analytical solutions, it gives inaccurate results for at least two cases. First, in the case of no elastic mismatch, the formula predicts that $Z_d \to 0.748$ as $d/h_f \to 0$, about 25% lower than the analytical solution. Second, the interfacial energy release rates for intermediate crack lengths by the approximate formula in general do not compare closely with numerical results, especially for cases with $\alpha < 0$, where the oscillation and the maxima are not well captured by the approximation. As will be discussed later, the maximum interfacial energy release rate for $\alpha \le 0$ is critical for determining the condition of interfacial delamination along side the channel crack. Another previous study by Yu et al. (2001) investigated interfacial delamination under two different edge conditions. While the steady-state interfacial energy

release rate is the same for all edge conditions, the short crack limit strongly depends on the edge effect.

A necessary condition for steady-state channel cracking with concomitant interfacial delamination is that the interfacial crack arrests at a finite width. The delamination width can be determined by comparing the interfacial energy release rate in Eq. (4) to the interface toughness. In general, the interface toughness depends on the phase angel of mode mix (Hutchinson and Suo, 1992), which in turn depends on the delamination width, as shown in Figure 4. Due to the oscillatory nature of the stress singularity at the interfacial crack tip (Rice, 1988), a length scale has to be used to define the phase angle. Here we take the film thickness h_f as the length scale, and define the mode angle as

$$\psi = \tan^{-1}\left(\frac{\mathrm{Im}\left(Kh_f^{i\varepsilon}\right)}{\mathrm{Re}\left(Kh_f^{i\varepsilon}\right)}\right), \tag{8}$$

where $K = K_1 + iK_2$ is the complex stress intensity factor, and $\varepsilon = \frac{1}{2\pi}\ln\left(\frac{1-\beta}{1+\beta}\right)$. The real and imaginary parts of the complex stress intensity factor are calculated by the interaction integral method in ABAQUS. Figure 4 shows that the phase angle quickly approaches a steady state

$$\psi_{ss} = \omega(\alpha, \beta), \tag{9}$$

as given by Suo and Hutchinson (1990). When the film and the substrate have identical elastic moduli ($\alpha = \beta = 0$), we have $\psi_{ss} = \omega(0,0) = 52^\circ$. Considering the fact that the variation of the phase angle with respect to the delamination width is relatively small and confined within a small range of short cracks ($d < h_f$), we take the constant steady-state phase angle, Eq. (9), in the subsequent discussions and assume that the interface toughness is independent of the

delamination width, i.e., $\Gamma_i = \Gamma_i(\psi_{ss})$. Then, the width of the interfacial delamination can be determined by requiring that

$$Z_d\left(\frac{d_s}{h_f}, \alpha, \beta\right) = \overline{\Gamma}_i = \frac{\overline{E}_f \Gamma_i(\psi_{ss})}{\sigma_f^2 h_f}. \tag{10}$$

The right-hand side of Eq. (10) is the normalized interface toughness, independent of the interfacial crack length. In the following, we discuss possible solutions to Eq. (10) for different elastic mismatches.

First, when $\alpha = \beta = 0$ (i.e., no elastic mismatch), the Z_d function has a maximum, $Z_d \to 0.9878$ as $d/h_f \to 0$, and it approaches the steady state, $Z_d \to 0.5$, for long cracks. Consequently, when $\overline{\Gamma}_i \geq 0.9878$ (strong interface), the interfacial energy release rate is always lower than the interface toughness, and thus no delamination would occur (i.e., $d_s = 0$). On the other hand, when $\overline{\Gamma}_i \leq 0.5$ (weak interface), the interfacial energy release rate is always higher than the interface toughness. In this case, the interfacial crack would grow unstably to infinity (i.e., $d_s \to \infty$), causing spalling of the film from the substrate, unless the interfacial crack is arrested by other features such as geometric edges or material junctions. Only for an intermediate interface toughness with $0.9878 > \overline{\Gamma}_i > 0.5$, Eq. (10) has a finite solution, $0 < d_s < \infty$, in which case the channel crack grows with concomitant interfacial delamination of the width d_s. The stable delamination width is plotted as a function of the normalized interface toughness $\overline{\Gamma}_i$ in Figure 5.

Next, when $\alpha > 0$ (i.e., a stiff film on a relatively compliant substrate), the Z_d function is unbounded as $d/h_f \to 0$. Thus, for all interfaces with $\overline{\Gamma}_i > 0.5$, a stable delamination width d_s

can be obtained from Eq. (10). This indicates that interfacial delamination would always occur concomitantly with the channel crack when the substrate is more compliant than the film. As shown in Figure 5, the delamination width increases as the normalized interface toughness decreases. When $\overline{\Gamma}_i \le 0.5$, the interfacial crack grows unstably and the delamination width approaches infinity.

When $\alpha < 0$ (i.e., a compliant film on a relatively stiff substrate), the Z_d function necessarily starts from zero at $d/h_f = 0$, but has a local maximum (Z_{dm}) before it approaches the steady state value. The value Z_{dm} decreases as α decreases, which is greater than 0.5 when $0 > \alpha > -0.89$ and lower than 0.5 when $\alpha \le -0.89$. Consequently, when $0 > \alpha > -0.89$, no interfacial delamination occurs if $\overline{\Gamma}_i \ge Z_{dm}$, and stable delamination if $0.5 < \overline{\Gamma}_i < Z_{dm}$. On the other hand, when $\alpha \le -0.89$, stable delamination cannot occur; the channel crack either has no delamination for $\overline{\Gamma}_i \ge 0.5$ or causes unstable delamination for $\overline{\Gamma}_i < 0.5$. The stability of the interfacial delamination is dictated by the trend of the interfacial energy release rate with respect to the delamination width (Fig. 3). Although Eq. (10) has a finite solution for $\alpha < 0$ and $\overline{\Gamma}_i < 0.5$, the interfacial crack is unstable because $\frac{\partial Z_d}{\partial d} > 0$ (the minor oscillation of the Z_d function has been ignored here). Moreover, for both the stable and unstable delamination, a critical defect size is required for the initiation of the interfacial delamination, since the energy release rate approaches zero for very short cracks ($d/h_f \to 0$). This sets a barrier for the initiation of interfacial delamination from the channel crack when the substrate is mechanically stiffer than the film.

The above discussion is summarized in Figure 6 as an interfacial delamination map for different combinations of film/substrate elastic mismatch and interface toughness. Three regions are identified for (I) no delamination, (II) stable delamination, and (III) unstable delamination. In regions II and III, sub-regions for delamination without and with an initiation barrier are denoted by A and B, respectively. The boundary between Region I and Region II-B is determined from the present finite element calculations, corresponding the maximum interfacial energy release rate for $0 > \alpha > -0.89$. In an experimental study by Tsui et al. (2005), no interfacial delamination was observed for channel cracking of a low k film directly deposited on a Si substrate, while a finite delamination was observed when a polymer buffer layer was sandwiched between the film and the substrate. These observations are consistent with the delamination map. In the former case, the elastic mismatch between the film and the substrate, $\alpha = -0.91$, thus no delamination when the normalized interface toughness $\overline{\Gamma}_i \geq 0.5$ (i.e., Region I in Figure 6). With a polymer buffer layer, however, the elastic mismatch between the low k material and the polymer is, $\alpha = 0.4$. Although the polymer layer is relatively thin, it qualitatively changes the interfacial behavior from that for $\alpha < 0$ (Region I) to that for $\alpha > 0$ (Region II-A). More experimental evidences with different combinations of elastic mismatch, interface toughness, and film stress would be needed for further validation of the predicted delamination map.

4. Channel cracking with stable delamination

As the question regarding the occurrence of interfacial delamination from the root of a channel crack is addressed in the previous section, the next question is: how would the interfacial delamination influence the driving force for the growth of a channel crack? Again, we consider the steady-state growth. With a stable delamination along each side of the channel crack (Figure

2a), the substrate constraint on the opening of the channel crack is relaxed. Consequently, the steady-state energy release rate calculated from Eq. (3) becomes greater than Eq. (1). A dimensional consideration leads to

$$G_{ss}^{*} = Z^{*}\left(\frac{d}{h_f}, \alpha, \beta\right)\frac{\sigma_f^2 h_f}{\bar{E}_f}, \tag{11}$$

where Z^{*} is a new dimensionless coefficient that depends on the width of interfacial delamination (d/h_f) in addition to the elastic mismatch parameters. From an energetic consideration, we obtain that

$$G_{ss}^{*} = G_{ss} + \frac{2}{h_f}\int_0^d G_d(a)da, \tag{12}$$

where G_{ss} is the steady-state energy release rate of the channel crack with no delamination as given in Eq. (1), and $G_d(a)$ is the energy release rate of the interfacial crack of width *a* as given in Eq. (4). When $d/h_f \to 0$, $G_{ss}^{*} \to G_{ss}$ or $Z^{*} \to Z$, recovering Eq. (1); when $d/h_f \to \infty$, $Z^{*} \to \infty$. Furthermore, as $d_s/h_f \to \infty$, since the interfacial crack approaches the steady state ($G_d \to G_{ss}^{d}$ and $Z_d \to 0.5$), the increase of the energy release rate is simply

$$\Delta G_{ss}^{*} = \frac{2}{h_f}G_{ss}^{d}\Delta d \text{ , or } \Delta Z^{*} = \frac{\Delta d}{h_f}, \tag{13}$$

which dictates that the coefficient Z^{*} increases with the normalized delamination width d/h_f linearly with a slope of 1 at the limit of long delamination.

The same finite element model as illustrated in Figure 2 is employed to calculate Z^{*}, by integrating the opening displacement along the surface of the channel crack as Eq. (3). Figure 7

plots the difference, $Z^* - Z$, as a function of d/h_f for different elastic mismatch parameters. For a compliant film on a relative stiff substrate ($\alpha < 0$), the increase due to interfacial delamination is almost linear for the entire range of delamination width. For a stiff film on a relatively compliant substrate ($\alpha > 0$), however, the increase is nonlinear for short interfacial delamination and then approaches a straight line of slope 1 as predicted by Eq. (13). Apparently, with interfacial delamination, the driving force for channel cracking can be significantly higher than that assuming no delamination.

As discussed in the previous section, the stable delamination width, d_s/h_f, can be obtained as a function of the normalized interface toughness, $\overline{\Gamma}_i$, by Eq. (10), as shown in Figure 5. Thus, the coefficient Z^* in Eq. (11) may also be plotted as a function of $\overline{\Gamma}_i$, as shown in Figure 8. When $\alpha > 0$, $Z^* \to Z$ as $\overline{\Gamma}_i \to \infty$, and $Z^* \to \infty$ as $\overline{\Gamma}_i \to 0.5$; in between, Z^* increases as $\overline{\Gamma}_i$ decreases, because the interfacial delamination width increases. When $\alpha = 0$, $Z^* = Z$ as $\overline{\Gamma}_i \geq 0.9878$ (i.e., no delamination). When $0 > \alpha > -0.89$, Z^* increases from Z to infinity within a narrow window of $\overline{\Gamma}_i$, where stable delamination is predicted (Region II-B in Figure 6). For $\alpha < -0.89$, either $Z^* = Z$ for no delamination or $Z^* \to \infty$ for unstable delamination. Therefore, Figure 8 explicitly illustrates the influence of the interface toughness on the driving force of channel cracking in the film.

While the interfacial delamination, if occurring, relaxes the constraint on crack opening thus enhances the fracture driving force, it also requires additional energy to fracture the interface as the channel crack advances. An energetic condition can thus be stated: if the increase in the energy release exceeds the fracture energy needed for delamination, growth of the channel crack with interfacial delamination is energetically favored; otherwise, the channel crack grows with

no delamination. It can be shown that this condition is consistent with the delamination map in Figure 6. Considering the interfacial fracture energy, a fracture condition for steady-state growth of a channel crack can be written as

$$G_{ss}^{*} \geq \Gamma_f + W_d \,, \tag{14}$$

where Γ_f is the cohesive fracture toughness of the film, and W_d is the energy required to delaminate the interface accompanying per unit area growth of the channel crack. For stable delamination of width $d = d_s$ at both sides of a channel crack, the delamination energy is

$$W_d = \frac{2}{h_f}\int_0^{d_s} \Gamma_i\left(\psi(a)\right)da \approx 2\Gamma_i\left(\psi_{ss}\right)\frac{d_s}{h_f}\,. \tag{15}$$

Again, the phase angle of the interfacial crack is approximately taken as a constant independent of the crack length. When $d_s = 0$, Eq. (14) recovers the condition for cohesive fracture of the film, i.e., $G_{ss} \geq \Gamma_f$.

Equation (14) may not be convenient to apply directly, since both sides of the equation (driving force and resistance, respectively) increase with the interfacial delamination. By moving W_d to the left hand side and noting that the stable delamination width is a function of the interface toughness, we define an effective driving force for the steady-state channel cracking:

$$G_{ss}^{eff} = G_{ss}^{*} - W_d = Z_{eff}\left(\overline{\Gamma}_i, \alpha, \beta\right)\frac{\sigma_f^2 h_f}{\overline{E}_f}\,. \tag{16}$$

with

$$Z_{eff} = Z^{*}\left(\frac{d_s}{h_f}, \alpha, \beta\right) - 2\overline{\Gamma}_i\frac{d_s}{h_f}\,. \tag{17}$$

Using the effective energy release rate, the condition for the steady-state channel cracking is simply a comparison between G_{ss}^{eff} and Γ_f, the latter being a constant independent of the interface. Figure 9 plots the ratio, $Z_{eff}/Z(\alpha,\beta)$, as a function of $\overline{\Gamma}_i$ for different elastic mismatch parameters. At the limit of high interface toughness ($\overline{\Gamma}_i \to \infty$), $d_s \to 0$ and $Z_{eff} \to Z$, which recovers the case of channel cracking with no delamination. The effective driving force increases as the normalized interface toughness deceases. Compared to Figure 8, the influence of interfacial delamination on the effective driving force is reduced after considering the interfacial fracture energy.

5. Summary

This paper considers concomitant interfacial delamination and channel cracking in elastic thin films. Two main conclusions are summarized as follows.

- Stable interfacial delamination along a channel crack is predicted for certain combinations of film/substrate elastic mismatch, interface toughness, and film stress, as summarized in a delamination map (Figure 6), together with conditions for no delamination and unstable delamination.
- Interfacial delamination not only increases the fracture driving force for steady-state growth of the channel crack, but also adds to the fracture resistance by requiring additional energy for the interfacial fracture. An effective energy release rate for channel cracking is defined, which depends on the interface toughness (Figure 9) in addition to the elastic mismatch and can be considerably higher than the energy release rate assuming no delamination.

In particular, it is predicted that channel cracking in an elastic thin film on a relatively compliant substrate is always accompanied by interfacial delamination, either stable or unstable, depending on the interface toughness. This differs from the case for an elastic film on a relatively stiff substrate, in which channel cracks may grow without interfacial delamination (Region I in Figure 6). This difference may have important implications for reliability of integrated structures. As an example, for interconnect structures in microelectronics, the low-k dielectrics is usually more compliant compared to the surrounding materials (Liu et al., 2004). Therefore, fracture of the low-k dielectrics by channel cracking is typically not accompanied by interfacial delamination. However, when a more complaint buffer layer is added adjacent to the low-k film, interfacial delamination can occur concomitantly with channel cracking of the low-k film (Tsui et al., 2005). Moreover, a relatively stiff cap layer (e.g., SiN) is often deposited on top of the low-k film (Liu et al., 2007). Channel cracking of the cap layer on low-k could be significantly enhanced by interfacial delamination. Flexible electronics is another area of applications where compliant substrates have to be used extensively along with mechanically stiffer films for the functional devices and interconnects (Wagner et al., 2004; Khang et al., 2006). Here, interfacial delamination could play a critical role in the reliability assessment. As shown in a previous study by Li and Suo (2007), the stretchability of metal thin-film interconnects on a compliant substrate can be dramatically reduced by interfacial delamination. For brittle thin films on compliant substrates, as considered in the present study, interfacial delamination has a similar effect on the fracture and thus deformability of the devices.

Acknowledgments

This work is supported by the National Science Foundation through Grant No. 0546409.

Appendix: Short delamination crack from a channel root

This Appendix summarizes asymptotic solutions from previous studies (He and Hutchinson, 1989a & 1989b; Hutchinson and Suo, 1992) for short delamination cracks emanating from the root of a channel crack (i.e., $d/h_f \to 0$ in Figure 2a), and presents comparisons with numerical results from the finite element model shown in Figure 2.

A.1 Zero elastic mismatch ($\alpha = \beta = 0$)

This is a case of crack kinking in a homogeneous solid. Without the interfacial delamination, the channel crack in the film is equivalent to a two-dimensional edge crack, with the stress intensity factor at the root

$$K_I = 1.1215\sigma_f \sqrt{\pi h_f} \ . \tag{A1}$$

For a small crack segment ($d << h_f$) kinking out of the plane of the edge crack, the stress intensity factors at the new crack tip are linearly related to the stress intensity factors at the tip of the parent crack (Hutchinson and Suo, 1992), namely

$$\begin{aligned} K_I^d &= c_{11}K_I + c_{12}K_{II} \\ K_{II}^d &= c_{21}K_I + c_{22}K_{II} \end{aligned}, \tag{A2}$$

where the coefficients, c_{ij}, depend on the kink angle, as given by Hayashi and Nemat-Nasser (1981). Following He and Hutchinson (1989b), the coefficients can be written as

$$c_{11} = C_R + D_R \,,\ c_{21} = C_I - D_I \,, \tag{A3}$$

where $C = C_R + iC_I$ and $D = D_R + iD_I$ are two complex valued functions, with the subscripts R and I denoting their real and imaginary parts, respectively. An approximation by Cotterell (1965) gives that

$$C = \frac{1}{2}\left(e^{-i\omega/2} + e^{-i3\omega/2}\right),\ D = \frac{1}{4}\left(e^{-i\omega/2} - e^{i3\omega/2}\right), \tag{A4}$$

where ω is the kink angle. Cotterell and Rice (1980) have shown that this approximation is asymptotically correct for small kink angles and is reasonably accurate for kink angles as large as 45° or even 90°, depending on the mode mix.

For the present problem with a channel crack kinking into the interface, the kink angle is 90° and $K_{II} = 0$. Under the plane strain condition, the energy release rate of the interfacial crack is

$$G_d\left(d \to 0\right) = \frac{\left(K_I^d\right)^2 + \left(K_{II}^d\right)^2}{\overline{E}} = \left(1.1215\right)^2 \pi\left(c_{11}^2 + c_{21}^2\right)\frac{\sigma_f^2 h_f}{\overline{E}}. \tag{A5}$$

A comparison between Eq. (A5) and Eq. (4) gives the dimensionless coefficient

$$Z_d\left(d \to 0\right) = 1.258\pi\left(c_{11}^2 + c_{21}^2\right). \tag{A6}$$

Using the approximation (A4) with $\omega = \pi/2$, we obtain that

$$c_{11} = \frac{\sqrt{2}}{4},\ c_{21} = -\frac{\sqrt{2}}{4}. \tag{A7}$$

Inserting (A7) into (A6) gives that

$$Z_d\left(d \to 0\right) = 0.9878. \tag{A8}$$

This approximation agrees well with the numerical result shown in Figure 3, where $Z_d = 0.9923$ for $d/h_f = 10^{-3}$.

A.2 Crack deflection at a bimaterial interface

For an interface between two elastic materials with general elastic mismatch, an asymptotic solution by He and Hutchinson (1989a) gives the energy release rate of the delamination crack emanating from a perpendicular channel crack (Figure 2a, $d << h_f$):

$$G_d = \left(\frac{1}{\overline{E}_f} + \frac{1}{\overline{E}_s}\right)\frac{K_1^2 + K_2^2}{2\cosh^2 \pi\varepsilon} = \left(\frac{1}{\overline{E}_f} + \frac{1}{\overline{E}_s}\right)\frac{k_1^2[|C|^2 + |D|^2 + 2\mathrm{Re}(CD)]}{2\cosh^2 \pi\varepsilon} d^{1-2\lambda}. \quad \text{(A9)}$$

where C and D are dimensionless, complex valued functions of α and β, k_1 is a real valued constant representing the stress intensity at the root of the channel crack, and λ is determined by Eq. (7). This asymptotic solution leads to a power-law dependence of the Z_d function on the interfacial crack length as $d \to 0$, namely

$$Z_d = \frac{G_d}{\sigma_f^2 h_f / \overline{E}_f} \sim \left(\frac{d}{h_f}\right)^{1-2\lambda} . \quad \text{(A10)}$$

Figures A1 and A2 plot the numerical solutions of Z_d from the finite element model (Figure 2), in comparison with the asymptotic solution. When $\alpha < 0$ ($\beta = \alpha/4$), $0 < \lambda < 0.5$ and the log-log plot of Z_d vs d/h_f (Figure A1) approaches a straight line of positive slope $(1-2\lambda > 0)$ as $d/h_f \to 0$. When $\alpha > 0$, $\lambda > 0.5$ and the log-log plot (Figure A2) approaches a straight line of negative slope $(1-2\lambda < 0)$. When $\alpha = \beta = 0$ (no elastic mismatch), $\lambda = 0.5$ and Z_d approaches a constant with zero slope in the log-log plot (Figure A2). The comparisons show good agreement between the numerical results and the asymptotic power law for short delamination cracks.

References

Ambrico JM, Begley MR (2002) The role of initial flaw size, elastic compliance and plasticity in channel cracking of thin films. Thin Solid Films **419**: 144-153.

Beuth JL (1992) Cracking of thin bonded film in residual tension. Int. J. Solids Struct. **29**: 63-191.

Cordero N, Yoon J, Suo Z (2007) Channel cracks in hermetic coating consisting of organic and inorganic layers. Appl. Phys. Lett. **90**: 111910.

Cotterell B (1965) On brittle fracture paths. Int. J. Fracture Mech. **1**: 96-103.

Cotterell B, Rice JR (1980) Slightly curved or kinked cracks. Int. J. Fracture **16**: 155-169.

Dodabalapur A (2006) Organic and polymer transistors for electronics. Materials Today 9: 24-30.

Gao H (2006) Application of fracture mechanics concepts to hierarchical biomechanics of bone and bone-like materials. Int. J. Fracture 138: 101–137.

Hayashi K, Nemat-Nasser S (1981) Energy-release rate and crack kinking under combined loading. J. Appl. Mech. **48**: 520-524.

He J, Xu G, Suo Z (2004) Experimental determination of crack driving forces in integrated structures. Proc. 7th Int. Workshop on Stress-Induced Phenomena in Metallization (Austin, Texas, 14-16 June 2004), pp. 3-14.

He MY, Hutchinson JW (1989a) Crack deflection at an interface between dissimilar elastic materials. Int. J. Solids Struct. **25**: 1053-1067.

He MY, Hutchinson JW (1989b) Kinking of a crack out of an interface. J. Appl. Mech. **56**: 270-278.

Ho PS, Wang G, Ding M, Zhao JH, Dai X (2004) Reliability issues for flip-chip packages. Microelectronics Reliability 44: 719-737.

Huang R, Prevost JH, Huang ZY, Suo Z (2003) Channel-cracking of thin films with the extended finite element method. Eng. Frac. Mech. **70**: 2513-2526.

Huang R, Prevost JH, Suo Z (2002) Loss of constraint on fracture in thin film structures due to creep. Acta Mater. **50**: 4137-4148.

Hutchinson JW, Suo Z (1992) Mixed mode cracking in layered materials. Advances in Applied Mechanics **29**: 63-191.

Khang DY, Jiang HQ, Huang Y, Rogers JA (2006). A stretchable form of single-crystal silicon for high-performance electronics on rubber substrate. Science 311: 208-212.

Li T, Suo Z (2007). Ductility of thin metal films on polymer substrates modulated by interfacial adhesion. International Journal of Solids and Structures **44**: 1696-1705.

Liu XH, Lane MW, Shaw TM, Liniger EG, Rosenberg RR, Edelstein DC (2004) Low-k BEOL mechanical modeling. Proc. Advanced Metallization Conference: 361-367.

Liu XH, Lane MW, Shaw TM, Simonyi E (2007) Delamination in patterned films. Int. J. Solids Struct. **44**: 1706-1718.

Nakamura T, Kamath SM (1992) Three-dimensional effects in thin-film fracture mechanics. Mech. Mater. **13**: 67-77.

Rice JR (1988) Elastic fracture concepts for interfacial cracks. J. Appl. Mech. **55**: 98-103.

Suo Z (2003) Reliability of Interconnect Structures. In Volume 8: Interfacial and Nanoscale Failure (W. Gerberich, W. Yang, Editors) of *Comprehensive Structural Integrity* (I. Milne, R.O. Ritchie, B. Karihaloo, Editors-in-Chief), Elsevier, Amsterdam, pp. 265-324.

Suo Z, Hutchinson JW (1990) Interface crack between two elastic layers. Int. J. Fracture **43**: 1-18.

Suo Z, Prevost JH, Liang J (2003) Kinetics of crack initiation and growth in organic-containing integrated structures. J. Mech. Phys. Solids **51**: 2169-2190.

Tsui TY, McKerrow AJ, Vlassak JJ (2005) Constraint effects on thin film channel cracking behavior. J. Mater. Res. **20**: 2266-2273.

Tsui TY, McKerrow AJ, Vlassak JJ (2006) The effect of water diffusion on the adhesion of organosilicate glass film stacks. J. Mech. Phys. Solids **54**: 887-903.

Wagner S, Lacour SP, Jones J, Hsu PI, Sturm J, Li T, Suo Z (2004) Electronic skin: architecture and components. Physica E 25: 326-334.

Ye T, Suo Z, Evans, AG (1992) Thin film cracking and the roles of substrate and interface. Int. J. Solids Struct. **29**: 2639-2648.

Yu HH, He MY, Hutchinson JW (2001) Edge effects in thin film delamination. Acta Mater. **49**: 93-107.

Zak AR, Williams ML (1963) Crack point stress singularities at a bi-material interface. J. Appl. Mech. 30: 142-143.

FIGURE CAPTIONS

Figure 1. (a) Illustration of a channel crack with no interfacial delamination; (b) a channel crack with symmetric interfacial delamination of width *d* on both sides far behind the channel front.

Figure 2. (a) Schematics of the 2D plane strain model of a steady-state channel crack with interfacial delamination; (b) geometry of the finite element model, with uniform normal traction (σ_f) acting onto the surface of the channel crack and a symmetry boundary condition for the substrate; (c) an example finite element mesh, with infinity elements along the bottom and right boundaries; (d) a detailed mesh around the tip of the interfacial crack.

Figure 3. Normalized energy release rate of interfacial delamination from the root of a channel crack as a function of the normalized delamination width for different elastic mismatch parameters.

Figure 4. Phase angle of the mode mix for interfacial delamination as a function of the normalized delamination width for different elastic mismatch parameters. The dashed line indicates of the steady-state phase angle (52°) for the case of zero elastic mismatch ($\alpha = \beta = 0$).

Figure 5. The normalized stable delamination width as a function of the normalized interface toughness $\overline{\Gamma}_i = \Gamma_i / \Sigma$, where $\Sigma = \sigma_f^2 h_f / \overline{E}_f$.

Figure 6. A map for interfacial delamination from the root of a channel crack ($\beta = \alpha/4$): (I) no delamination, (II) stable delamination, and (III) unstable delamination, where A and B denote delamination without and with an initiation barrier, respectively.

Figure 7. Increase of the driving force for steady-state channel cracking due to concomitant interfacial delamination.

Figure 8. Influence of the normalized interface toughness ($\Sigma = \sigma_f^2 h_f / \overline{E}_f$) on the steady-state driving force for channel cracking.

Figure 9. Effective driving force for steady-state channel cracking as a function of the normalized interface toughness ($\Sigma = \sigma_f^2 h_f / \overline{E}_f$).

Figure A1. Normalized energy release rate of interfacial delamination emanating from the root of a channel crack, for $\alpha = -0.99$ and $\alpha = -0.6$. The asymptotic power law, Eq. (A10), is represented by the straight lines at the short crack limit with slopes, $1 - 2\lambda = 0.376$ and 0.224, respectively.

Figure A2. Normalized energy release rate of interfacial delamination emanating from the root of a channel crack, for $\alpha = 0$, $\alpha = 0.2$, and $\alpha = 0.6$. The asymptotic power law, Eq. (A10), is represented by the straight lines at the short crack limit with slopes, $1 - 2\lambda = 0$, -0.084, and -0.308, respectively.

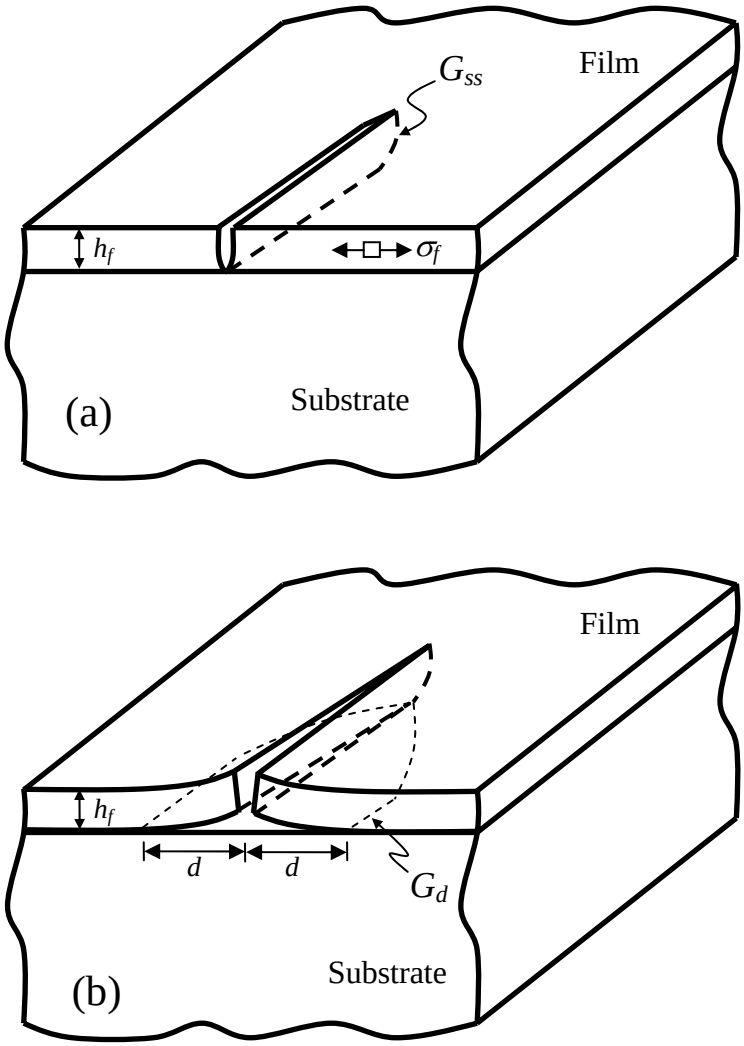

Figure 1. (a) Illustration of a channel crack with no interfacial delamination; (b) a channel crack with symmetric interfacial delamination of width *d* on both sides far behind the channel front.

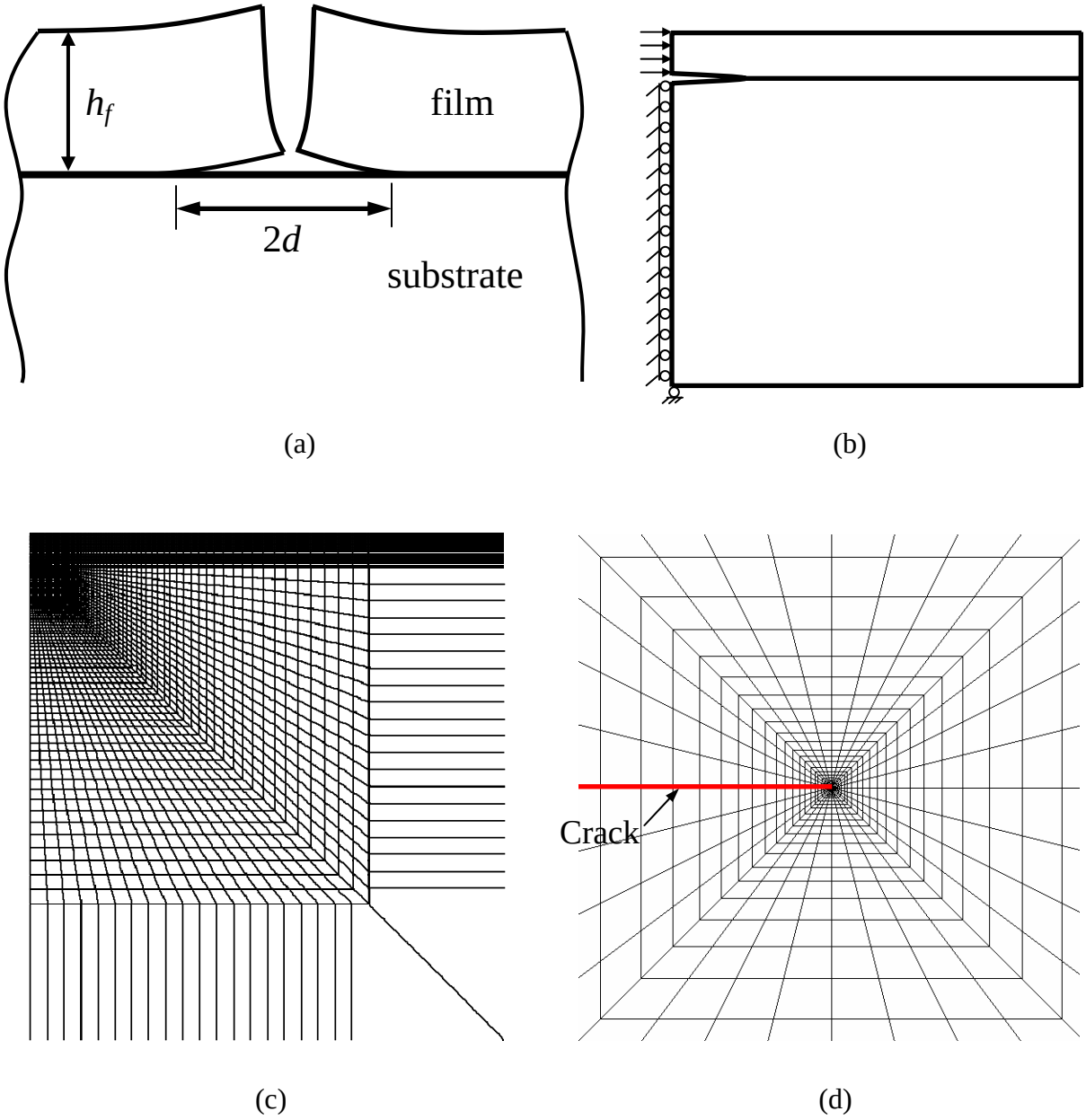

Figure 2. (a) Schematics of the 2D plane strain model of a steady-state channel crack with interfacial delamination; (b) geometry of the finite element model, with uniform normal traction (σ_f) acting onto the surface of the channel crack and a symmetry boundary condition for the substrate; (c) an example finite element mesh, with infinity elements along the bottom and right boundaries; (d) a detailed mesh around the tip of the interfacial crack.

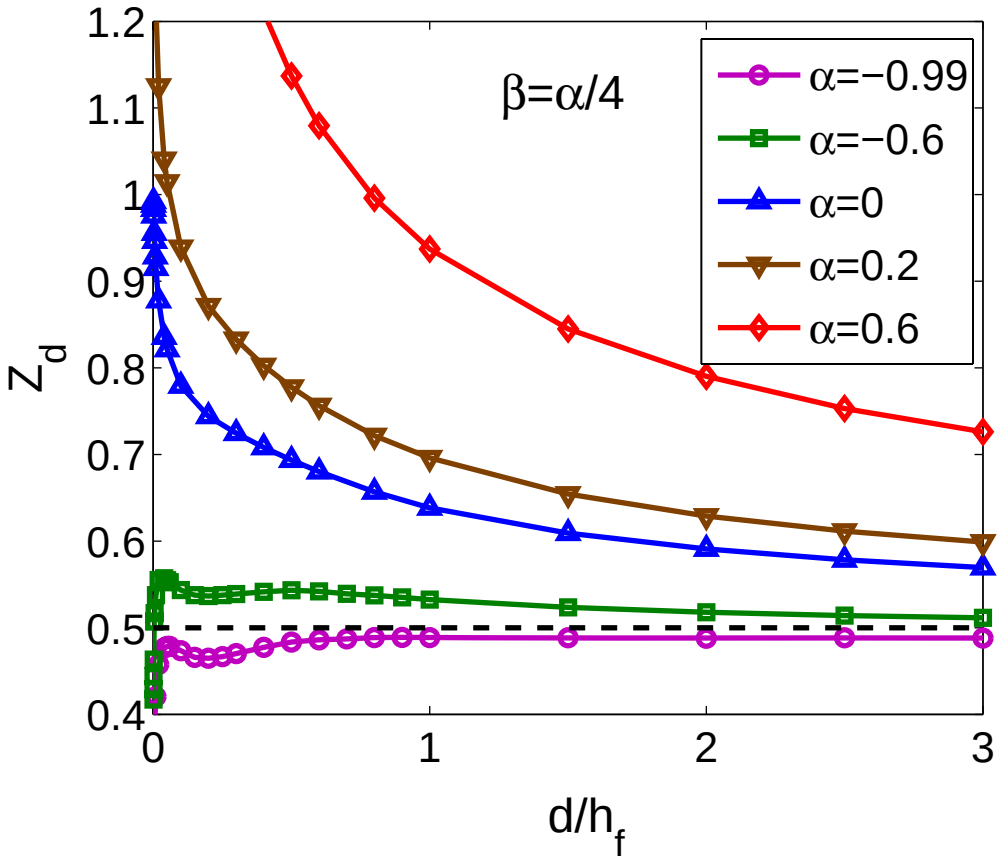

Figure 3. Normalized energy release rate of interfacial delamination from the root of a channel crack as a function of the normalized delamination width for different elastic mismatch parameters.

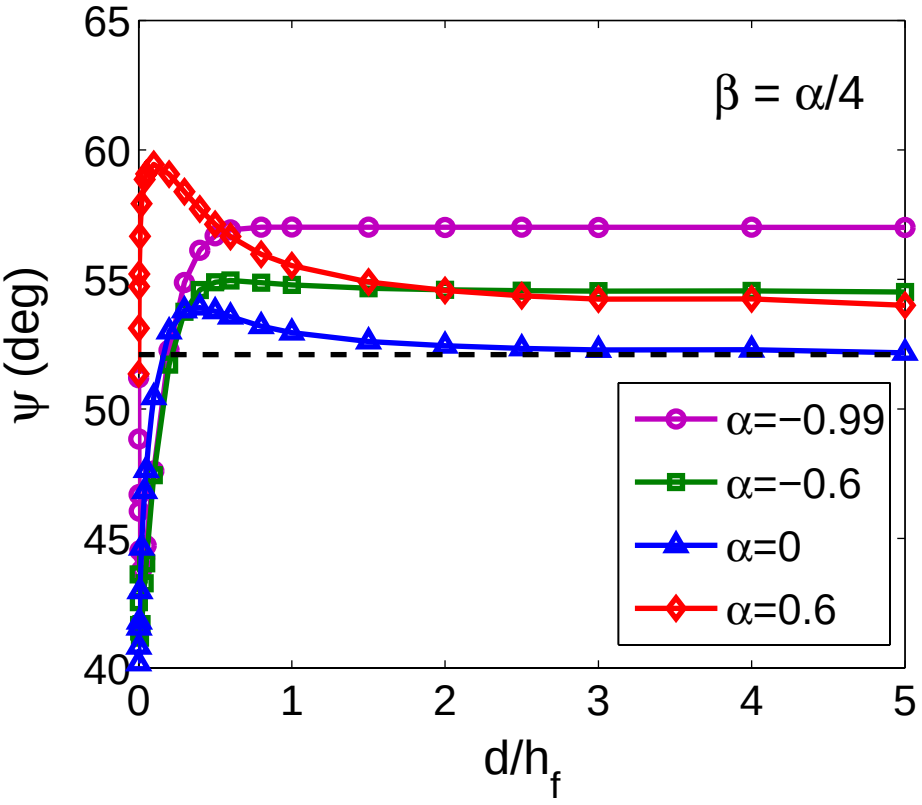

Figure 4. Phase angle of the mode mix for interfacial delamination as a function of the normalized delamination width for different elastic mismatch parameters. The dashed line indicates of the steady-state phase angle (52°) for the case of zero elastic mismatch ($\alpha = \beta = 0$).

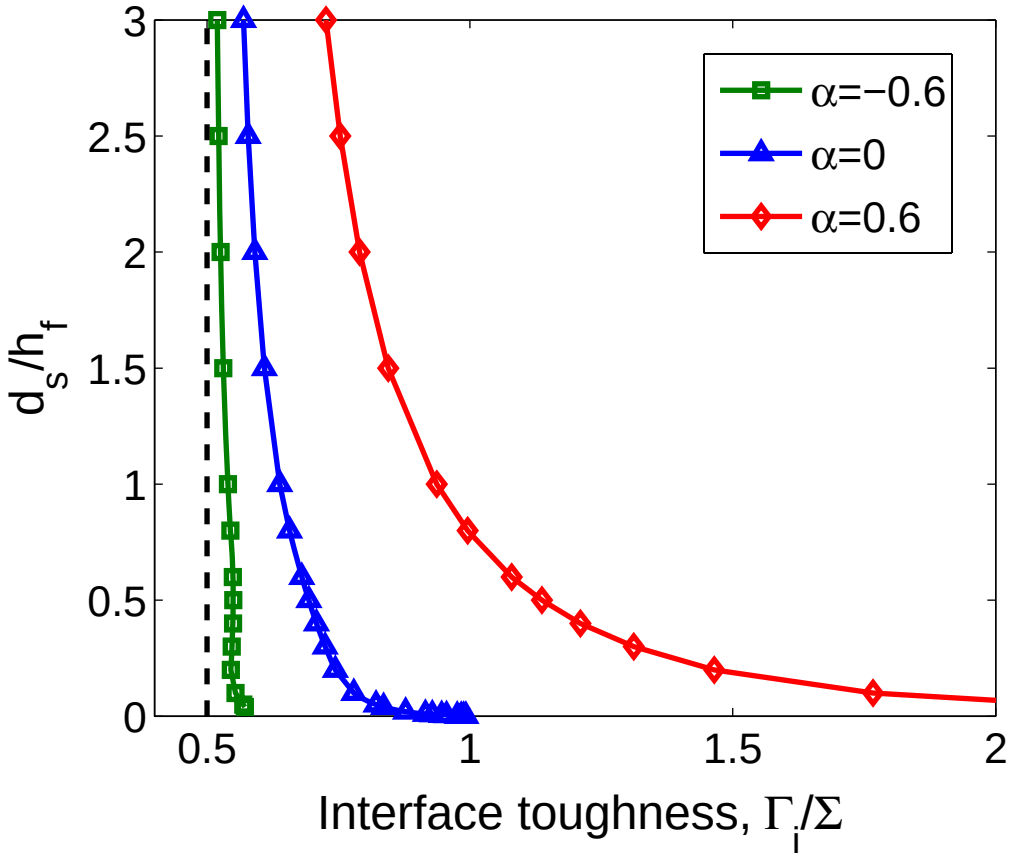

Figure 5. The normalized stable delamination width as a function of the normalized interface toughness $\bar{\Gamma}_i = \Gamma_i / \Sigma$, where $\Sigma = \sigma_f^2 h_f / \bar{E}_f$.

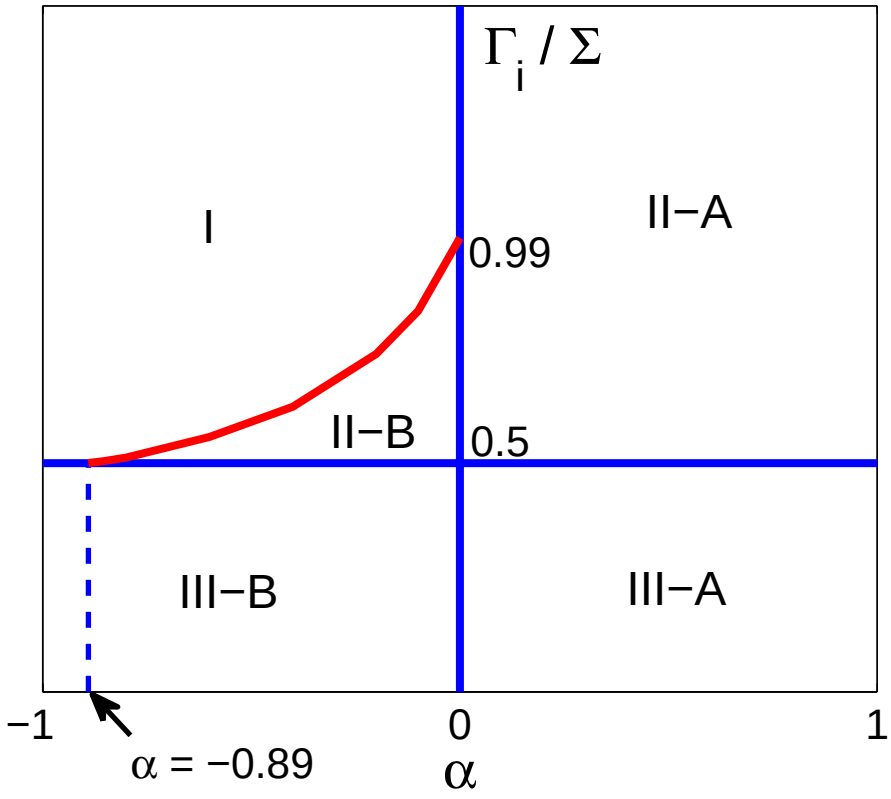

Figure 6. A map for interfacial delamination from the root of a channel crack ($\beta = \alpha/4$): (I) no delamination, (II) stable delamination, and (III) unstable delamination, where A and B denote delamination without and with an initiation barrier, respectively.

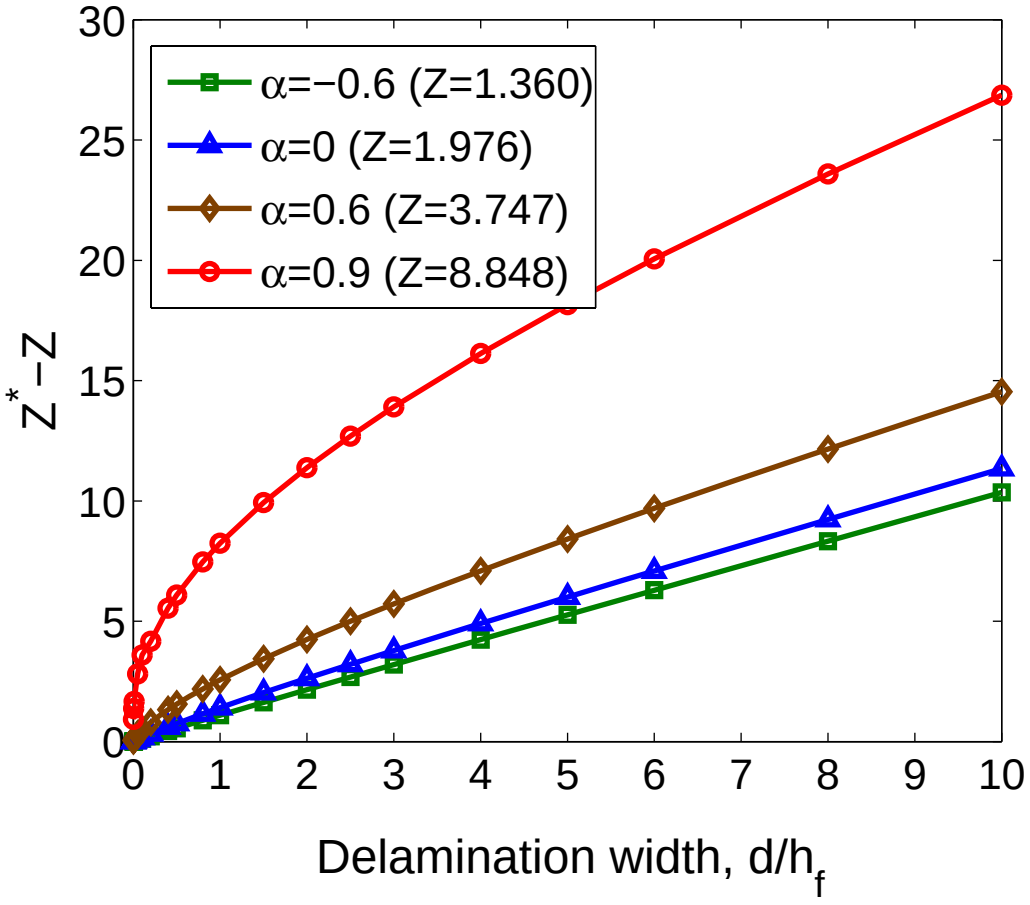

Figure 7. Increase of the driving force for steady-state channel cracking due to concomitant interfacial delamination.

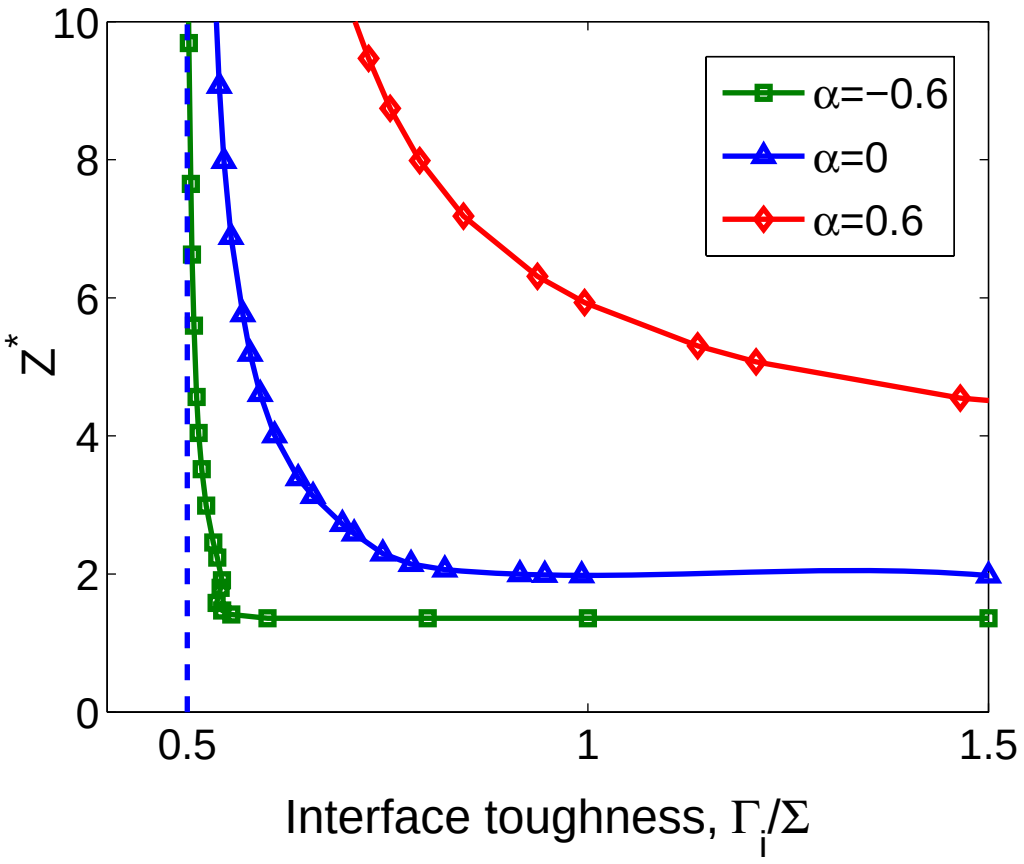

Figure 8. Influence of the normalized interface toughness ($\Sigma = \sigma_f^2 h_f / \overline{E}_f$) on the steady-state driving force for channel cracking.

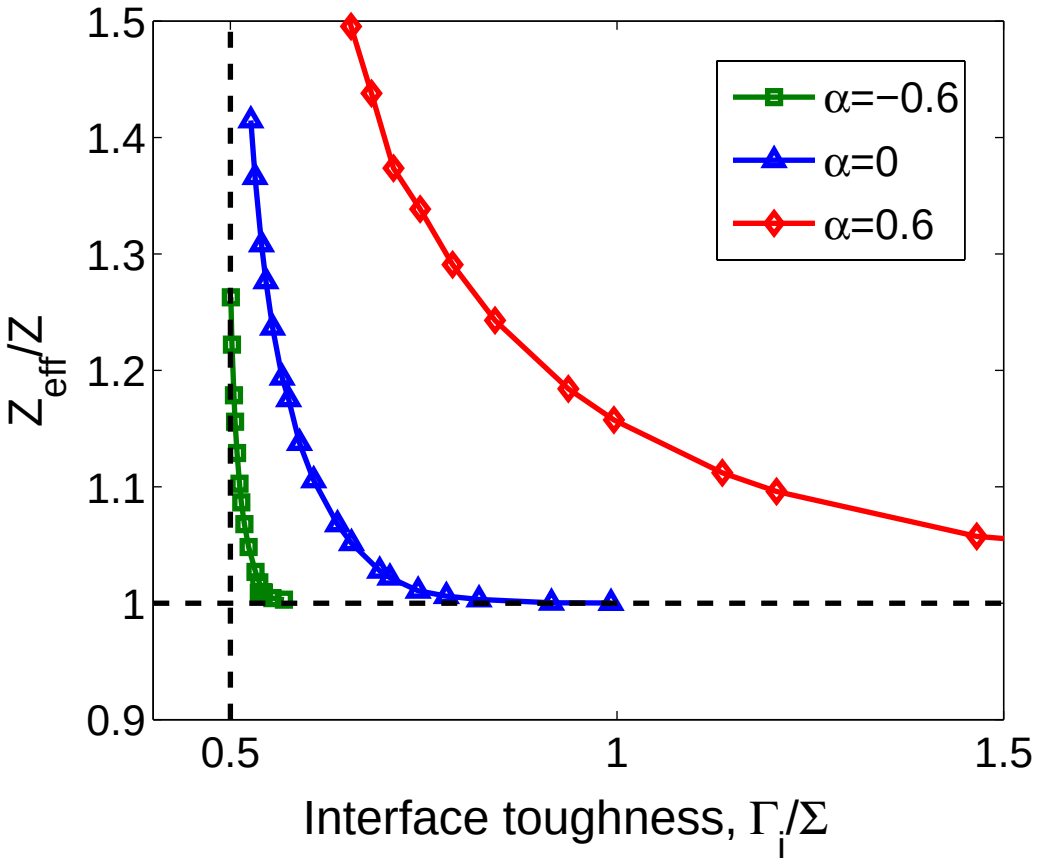

Figure 9. Effective driving force for steady-state channel cracking as a function of the normalized interface toughness ($\Sigma = \sigma_f^2 h_f / \overline{E}_f$).

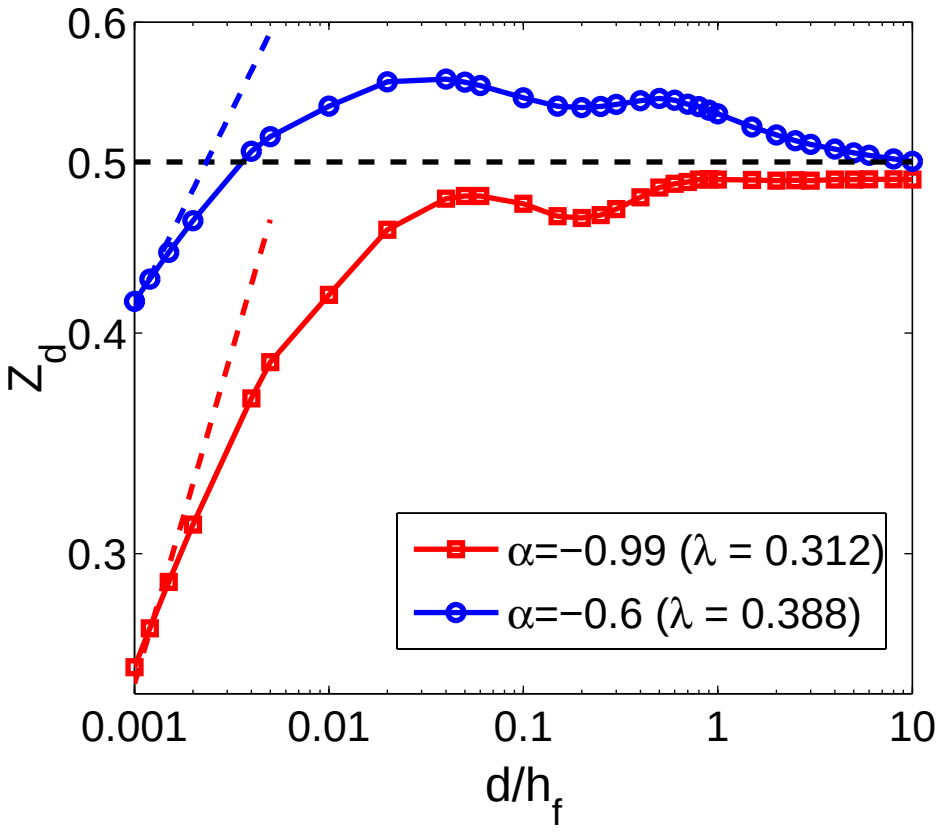

Figure A1. Normalized energy release rate of interfacial delamination emanating from the root of a channel crack, for $\alpha = -0.99$ and $\alpha = -0.6$. The asymptotic power law, Eq. (A10), is represented by the dashed straight lines at the short crack limit with slopes, $1-2\lambda = 0.376$ and 0.224, respectively.

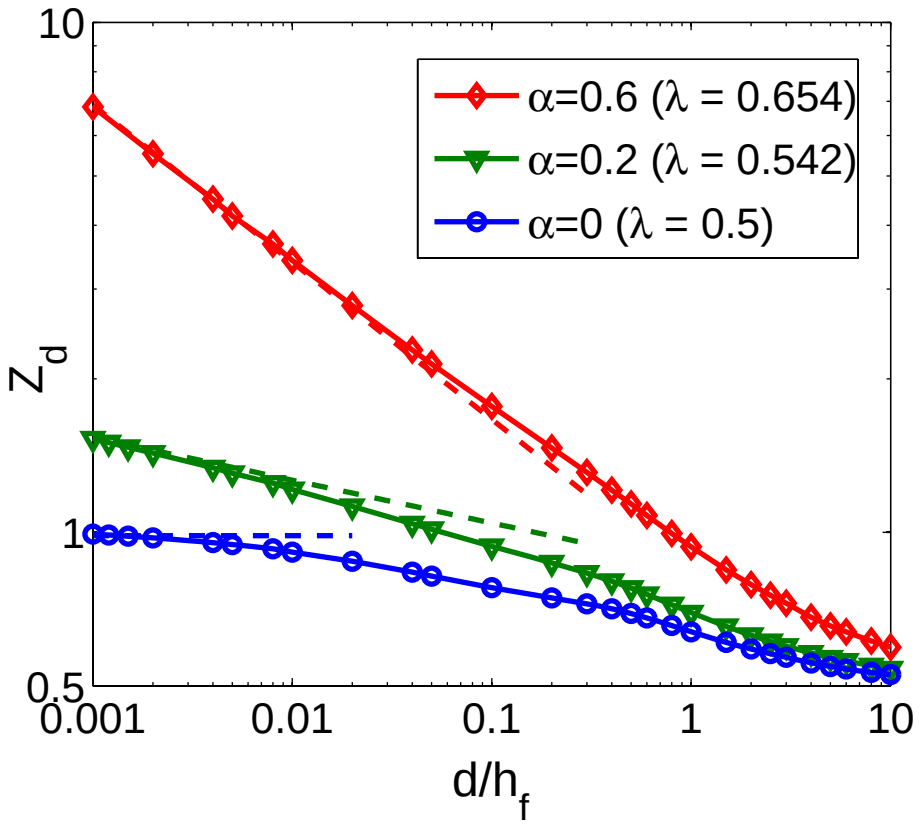

Figure A2. Normalized energy release rate of interfacial delamination emanating from the root of a channel crack, for $\alpha = 0$, $\alpha = 0.2$, and $\alpha = 0.6$. The asymptotic power law, Eq. (A10), is represented by the dashed straight lines at the short crack limit with slopes, $1-2\lambda = 0$, -0.084, and -0.308, respectively.